mathematics

IMPACT FACTOR 2.3

CITESCORE 4.0

Article

Riemann Problem for the Isentropic Euler Equations of Mixed Type in the Dark Energy Fluid

Tingting Chen, Weifeng Jiang, Tong Li, Zhen Wang and Junhao Lin

MDPI

https://doi.org/10.3390/math12162444

mathematics

MDPI

Article

Riemann Problem for the Isentropic Euler Equations of Mixed Type in the Dark Energy Fluid

Tingting Chen [1], Weifeng Jiang [2,*], Tong Li [3], Zhen Wang [4] and Junhao Lin [2]

[1] School of Mathematics and Computer Sciences, Jianghan University, Wuhan 430056, China; chenting0617@163.com
[2] Key Laboratory of Intelligent Manufacturing Quality Big Data Tracing and Analysis of Zhejiang Province, College of Science, China Jiliang University, Hangzhou 310018, China; jlyjssm2017@163.com
[3] Department of Mathematics, The University of Iowa, Iowa City, IA 52242, USA; tong-li@uiowa.edu
[4] Center for Mathematical Sciences, Department of Mathematics, Wuhan University of Technology, Wuhan 430070, China; zwang@whut.edu.cn
* Correspondence: casujiang89@cjlu.edu.cn

Abstract: We are concerned with the Riemann problem for the isentropic Euler equations of mixed type in the dark energy fluid. This system is non-strictly hyperbolic on the boundary curve of elliptic and hyperbolic regions. We obtain the unique admissible shock waves by utilizing the viscosity criterion. Assuming fixed left states are in the elliptic and hyperbolic regions, respectively, we construct the unique Riemann solution for the mixed-type models with the initial right state in some feasible regions. Finally, we present numerical simulations which are consistent with our theoretical results.

Keywords: conservation laws; Riemann problem; mixed type; shock waves

MSC: 35M10; 35M11; 83C56

Citation: Chen, T.; Jiang, W.; Li, T.; Wang, Z.; Lin, J. Riemann Problem for the Isentropic Euler Equations of Mixed Type in the Dark Energy Fluid. *Mathematics* **2024**, *12*, 2444. https://doi.org/10.3390/math12162444

Academic Editor: Xiangmin Jiao

Received: 9 July 2024
Revised: 3 August 2024
Accepted: 5 August 2024
Published: 6 August 2024

1. Introduction

In this paper, we consider the isentropic Euler equations of gas dynamics as follows:

$$\begin{cases} \rho_t + (\rho u)_x = 0, \\ (\rho u)_t + \left(\rho u^2 + p(\rho)\right)_x = 0, \end{cases} \quad (t, x) \in \mathbb{R}^+ \times \mathbb{R}, \tag{1}$$

with the equation of state (EoS)

$$p(\rho) = \rho \ln \rho, \quad \rho > 0, \tag{2}$$

where ρ, u, and p represent the density, the velocity, and the pressure, respectively [1]. System (1) with the EoS

$$p(\rho) = A\rho \ln(B\frac{\rho}{H^2}) + C\rho^2 + D\frac{1}{\rho} + E\rho \tag{3}$$

is called a dark energy fluid system, where A to E are constants, and H denotes the Hubble rate of our universe [2]. The use of a generalized dark energy EoS (3) makes possible the existence of de Sitter attractors, which has significant implications for understanding the nature of our universe. The dark energy fluid (3) is also used to describe the scenarios of dark matter–dark energy interaction [3]. In our work, we mainly study the Riemann solutions of dark energy (1) in terms of a logarithmic-corrected power-law fluid, that is, (2), which is a special form of (3) satisfying $A = B = H = 1$ and $C = D = E = 0$. It is

interesting that the EoS of (2) may have a deep relation with equations of state found in condensed matter fluids [4].

It is well known that the system (1) is the isentropic Euler equations of gas dynamics. The pressure $p(\rho)$ varies for different models. The system (1) for the ideal polytropic gas satisfies $p = p_0\rho^\gamma$, where $p_0 > 0$ and $\gamma \geq 1$ is the adiabatic exponent. It was well studied in [1,5–13]. If the pressure $p = -\frac{a}{\rho^\mu}$, $a > 0$, $\mu \in (0, 1]$, it is the generalized Chaplygin gas model in [14], which is a proposal to explain the origin of dark energy as well as dark matter through a single fluid. For $\mu = 1$, it is for the Chaplygin gas model, and δ-shock waves may occur for the Riemann problem [15]. With $p = A \ln \rho$, it has been introduced as a natural and robust candidate for a new unification of dark matter and dark energy [16]. It is also used to describe our universe filled with a single dark fluid [17]. For the above models, $p(\rho)$ is strictly increasing, which means that the system is globally hyperbolic. Noting that the isentropic Euler equations with the terms from (3), such as ρ^2, $-\frac{1}{\rho}$, and ρ, have been well studied, we are interested in the Riemann solutions for the isentropic Euler equations (1) with the EoS (2). To our knowledge, there are no related results. Since (2) is not monotonous any more, (1) and (2) are the isentropic Euler equations of mixed type.

The pathology of mixed-type systems concerns the ill-posedness [18] of the initial value problem. More precisely, there is no uniqueness of the Riemann problem if one considers the whole set of admissible solutions [19]. For example, the pressure of van der Waals fluid [20,21] is

$$p = \frac{RT}{v - b} - \frac{a}{v^2}, \tag{4}$$

where $v = \frac{1}{\rho}$ denotes the specific volume. Considering the Riemann data

$$(\rho, u)_{t=0} = \begin{cases} (\rho_l, u_l), x < 0, \\ (\rho_r, u_r), x > 0, \end{cases} \tag{5}$$

satisfying $\rho_l < \alpha < \beta < \rho_r$, where α and β are constants such that $p'(\rho) > 0$ for $\rho \notin [\alpha, \beta]$ and $p'(\rho) < 0$ for $\rho \in (\alpha, \beta)$, it was often used to study the phase transitions. In Lagrangian coordinates, (1) is transformed into

$$\begin{cases} v_t - u_x = 0, \\ u_t + p(v)_x = 0, \end{cases} \tag{6}$$

which is called a $p-$system. There exist multiple Riemann solutions for (4) and (6) with (5) because of the stationary shocks [22] or nonclassical shocks [23]. The nonclassical shocks violate the classic Lax entropy condition [24] and Liu entropy condition [25]. For more models which contain both hyperbolic and elliptic regions, the reader is referred to [26–36].

System (1) with (2) is hyperbolic for $\rho \geq 1/e$ and elliptic for $0 \leq \rho < 1/e$. It is different from the van der Waals fluid model [19,23]. There is only one hyperbolic region for (1) with (2). However, in van der Waals fluid, there are two hyperbolic regions $(0, \alpha]$ and $[\beta, +\infty)$ where the Riemann solvers preserve the kinetic function [19]. In addition, system (1) with (2) is also different from the hyperbolic conservation laws [37]. The Lax entropy condition and the Liu entropy condition may not make sense in an elliptic region. Thus, if the initial left state (5) is in the elliptic region, we need a new entropy condition to guarantee the uniqueness.

In this paper, we provide the viscosity admissibility criterion to pick the admissible shock waves when the initial states (5) are in the elliptic region. According to the monotonicity of density ρ in a travelling wave, we obtain an entropy condition which makes sense for the disconnected Hugoniot curve and self-interaction Hugoniot curve. If the initial states (5) are in the hyperbolic region, we obtain that it is equivalent to the classical Lax entropy condition. In addition, we obtain the unique Riemann solutions for the initial data in the feasible region. Finally, we present the numerical simulations for the solutions. The

Gibbs phenomenon [38] appears at the boundary of the shock wave in the Euler equations of mixed type.

The paper is organized as follows. In Section 2, we introduce some basic quantities and properties for (1) and (2). In Section 3, we obtain the Hugoniot curves by the Rankine–Hugoniot conditions. Then, we propose an entropy condition by the viscosity criterion to obtain the admissible shock waves. In Section 4, the rarefaction waves are obtained through the Riemann invariants. In Section 5, the unique Riemann solutions for the initial states (5) in the solvable regions are constructed by the elementary waves. In Section 6, we present numerical tests to verify our theoretical results. In Section 7, we give a discussion about further work. In Section 8, we give a conclusion.

2. Preliminaries

In this section, we introduce the basic quantities and properties for (1) and (2). For the smooth solution, we know that (1) is equal to the following equations:

$$\begin{cases} \rho_t + u\rho_x + \rho u_x = 0, \\ u_t + \frac{\ln\rho+1}{\rho}\rho_x + uu_x = 0. \end{cases} \tag{7}$$

The eigenvalues are

$$\lambda_1(\rho, u) = u - \sqrt{\ln\rho + 1},\ \lambda_2(\rho, u) = u + \sqrt{\ln\rho + 1}. \tag{8}$$

If $\rho \geq \frac{1}{e}$, the system is hyperbolic. In particular, if $\rho = \frac{1}{e}$, the system is non-strictly hyperbolic, that is, $\lambda_1\left(\frac{1}{e}, u\right) = \lambda_2\left(\frac{1}{e}, u\right) = u$. And if $0 < \rho < \frac{1}{e}$, the system is elliptic. Hereafter, we take $m = \rho u$. On the (ρ, m) plane, we divide the plane into four pieces as in Figure 1, where the elliptic region satisfies

$$E = \{(\rho, m) | 0 < \rho < \frac{1}{e}\},$$

and the hyperbolic region satisfies $H = H_1 \bigcup H_2 \bigcup H_3$ with

$$\begin{aligned} H_1 &= \{(\rho, m) | \rho \geq \frac{1}{e}, 0 < \lambda_1 < \lambda_2\}, \\ H_2 &= \{(\rho, m) | \rho \geq \frac{1}{e}, \lambda_1 < 0 < \lambda_2\}, \\ H_3 &= \{(\rho, m) | \rho \geq \frac{1}{e}, \lambda_1 < \lambda_2 < 0\}. \end{aligned}$$

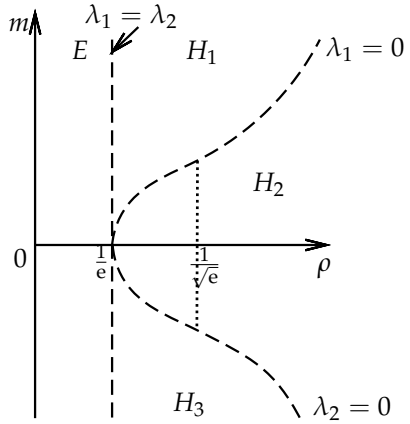

Figure 1. The elliptic region E and the hyperbolic regions H_1, H_2, and H_3.

The corresponding right vectors are

$$\vec{r}_1 = \left(-1, \frac{\sqrt{\ln\rho+1}}{\rho}\right)^T, \quad \vec{r}_2 = \left(1, \frac{\sqrt{\ln\rho+1}}{\rho}\right)^T. \tag{9}$$

According to

$$\nabla\lambda_1(\rho,u)\cdot\vec{r}_1 = \nabla\lambda_2(\rho,u)\cdot\vec{r}_2 = \frac{1}{2\rho\sqrt{\ln\rho+1}} + \frac{\sqrt{\ln\rho+1}}{\rho} > 0, \tag{10}$$

we know that this system (1) with (2) is genuinely nonlinear when the states are in the hyperbolic region. Moreover, according to the definition of the Riemann invariants [37] which satisfy $\nabla\omega_i\cdot\vec{r}_i = 0$, $i = 1,2$, we obtain the two Riemann invariants as follows:

$$\begin{cases} \omega_1 = \frac{m}{\rho} + \frac{2}{3}(\ln\rho+1)^{\frac{3}{2}}, \\ \omega_2 = \frac{m}{\rho} - \frac{2}{3}(\ln\rho+1)^{\frac{3}{2}}. \end{cases} \tag{11}$$

3. Shock Waves

In this section, we devote ourselves to the admissible shock waves. We first obtain the possible discontinuity curves in Section 3.1. Then, by the viscosity criterion, we propose the entropy condition (32) in Section 3.2. Finally, for the fixed left state (5) in different regions, we provide the shock wave curves and their properties on the (ρ, m) phase plane in Section 3.3.

3.1. Discontinuity Curves

Let $x(t)$ be the discontinuity curve. By the Rankine–Hugoniot (R-H) conditions [37],

$$\begin{cases} [\rho]\frac{\mathrm{d}x}{\mathrm{d}t} = [m], \\ [m]\frac{\mathrm{d}x}{\mathrm{d}t} = [\frac{m^2}{\rho} + p(\rho)], \end{cases} \tag{12}$$

where $[a] = a - a_l$, we have that if $[\rho] = 0$, then it holds that $[m] = 0$. The trivial solution is constant. If $[\rho] \neq 0$, we have that

$$[m]^2 = [\rho]\left[\frac{m^2}{\rho} + p(\rho)\right]. \tag{13}$$

It means that

$$\rho\rho_l\left(\frac{m}{\rho} - \frac{m_l}{\rho_l}\right)^2 = (\rho-\rho_l)(p(\rho)-p(\rho_l)), \tag{14}$$

which is called the Hugoniot curve. Thus, the right side of (14) should hold that

$$(\rho-\rho_l)(p(\rho)-p(\rho_l)) \geq 0. \tag{15}$$

We now discuss the sufficient condition of (15) with the fixed ρ_l. According to (2), we know that $p'(\rho) = \ln\rho + 1$ and $p''(\rho) = \frac{1}{\rho}$. Then, we depict the pressure p in Figure 2.

If $0 < \rho_l < 1$, there is always a ρ_l^* satisfying $p(\rho_l^*) = p(\rho_l)$, that is, $\rho_l^*\ln\rho_l^* = \rho_l\ln\rho_l$. From Figure 2, all the points satisfying $\rho > \rho_l^*$ make (15) hold. If the fixed $\rho_l \geq 1$, those points satisfying $\rho > \rho_l$ make (15) hold. Then, there are two discontinuity curves satisfying

$$\frac{m}{\rho} - \frac{m_l}{\rho_l} = \pm\sqrt{\frac{(\rho-\rho_l)(\rho\ln\rho - \rho_l\ln\rho_l)}{\rho\rho_l}}, \tag{16}$$

or

$$\frac{m-m_l}{\rho-\rho_l}=\frac{m_l}{\rho_l}\pm\sqrt{\frac{\rho(\rho\ln\rho-\rho_l\ln\rho_l)}{\rho_l(\rho-\rho_l)}}. \tag{17}$$

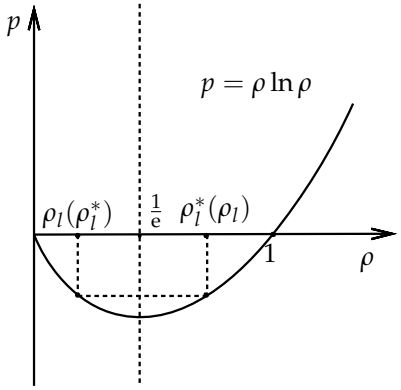

Figure 2. The picture of $p=\rho\ln\rho$, where $\rho_l^*\ln\rho_l^*=\rho_l\ln\rho_l$ when $0<\rho_l<1$.

We depict the Hugoniot curves (16) or (17) as in Figure 3 for three cases with ρ_l in different regions: (a) $0<\rho_l<\frac{1}{e}$, (b) $\frac{1}{e}\le\rho_l<1$, (c) $\rho_l\ge1$, respectively.

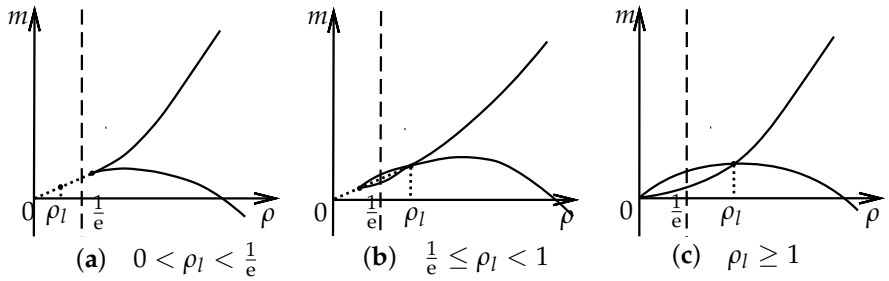

Figure 3. The Hugoniot curves with ρ_l in different regions. For case (**a**): $0<\rho_l<\frac{1}{e}$ and (**b**): $\frac{1}{e}\le\rho_l<1$; it holds that $\rho>\rho_l^*$. For case (**c**): $\rho_l\ge1$; it holds that $\rho>0$.

From Figure 3, if the initial left state is in the hyperbolic region, the Hugoniot curve of the mixed system (1) with (2) is not a simple curve. The initial left state is the self-intersection point of the Hugoniot curve. If the initial left state is in the elliptic region, the Hugoniot curve is not continuous. The initial left state is an isolated point.

3.2. Admissible Criterion

In this subsection, we consider the admissibility of the discontinuity curves by the viscosity criterion [39]. The viscosity system of (1) takes the form

$$\begin{cases}\rho_t+m_x=\varepsilon\rho_{xx},\\ m_t+\left(\frac{m^2}{\rho}+\rho\ln\rho\right)_x=0,\end{cases} \tag{18}$$

where ε is the assumed viscosity constant. Assume that $(s;\rho_l,m_l;\rho_r,m_r)$ satisfies the R-H conditions (12), where s denotes the shock speed. This discontinuity curve is said to be admissible according to the viscosity criterion if the wave is a limit as $\varepsilon\to0^+$ of the traveling wave solution $(P(\frac{x-st}{\varepsilon}),M(\frac{x-st}{\varepsilon}))$ of the system (18) with the boundary condition

$$(P(-\infty),M(-\infty);P(+\infty),M(+\infty))=(\rho_l,m_l;\rho_r,m_r), \tag{19}$$

where $(\rho_l, m_l; \rho_r, m_r)$ satisfies (16), $\rho_r \neq \rho_l$ and $\rho_r \geq \rho_l^*$. For simplicity of notation, we use ζ instead of $\frac{x-st}{\varepsilon}$. Then, the viscosity system (18) becomes

$$\begin{cases} P'(-s) + M' = P'', \\ M'(-s) + \left(\frac{M^2}{P} + P\ln P\right)' = 0, \end{cases} \tag{20}$$

where $' = \frac{\mathrm{d}}{\mathrm{d}\zeta}$. We have that

$$P'(-s^2) + \left(\frac{M^2}{P} + P\ln P\right)' = sP''. \tag{21}$$

The integration of the first equation of (20) and (21) from $-\infty$ to ζ coupled with (19) yields

$$\begin{cases} (P(\zeta) - \rho_l)(-s) + M(\zeta) - m_l = P'(\zeta), \\ (P(\zeta) - \rho_l)(-s^2) + \left(\frac{M^2}{P} + P\ln P\right)(\zeta) - c = sP'(\zeta), \end{cases} \tag{22}$$

where $c = \frac{m_l^2}{\rho_l} + \rho_l \ln \rho_l$. Then, we have the following result.

Lemma 1. *The traveling wave solution $P(\zeta)$ of (20), which connects the left state ρ_l and right state ρ_r, is strictly monotonous.*

Proof of Lemma 1. We now prove that there is no point such that $P'(\zeta) = 0$. Using proof by contradiction, we assume that there is a ζ_0 satisfying $P(\zeta_0) = P_0$ and $P'(\zeta_0) = 0$, where $P_0 \neq \rho_l, \rho_r$. Then, at ζ_0, we have that

$$(s - \frac{m_l}{\rho_l})^2 = \frac{P_0(P_0\ln P_0 - \rho_l \ln \rho_l)}{\rho_l(P_0 - \rho_l)} \tag{23}$$

by (22). Because of $P'(-\infty) = P'(+\infty) = 0$, it holds that

$$s = \frac{m_r - m_l}{\rho_r - \rho_l} \tag{24}$$

by the first equation of (22). Connected with (17), we have that

$$(s - \frac{m_l}{\rho_l})^2 = \frac{\rho_r(\rho_r \ln \rho_r - \rho_l \ln \rho_l)}{\rho_l(\rho_r - \rho_l)}. \tag{25}$$

Thus, by (23) and (25), it should hold that

$$\frac{\rho_r(\rho_r \ln \rho_r - \rho_l \ln \rho_l)}{\rho_r - \rho_l} = \frac{P_0(P_0 \ln P_0 - \rho_l \ln \rho_l)}{\rho_l(P_0 - \rho_l)}. \tag{26}$$

Let

$$G(\rho) = \frac{\rho(\rho \ln \rho - \rho_l \ln \rho_l)}{\rho - \rho_l}; \tag{27}$$

then, we know that

$$G'(\rho) = \frac{\rho(\ln \rho + 1) - \rho_l \frac{\rho \ln \rho - \rho_l \ln \rho_l}{\rho - \rho_l}}{\rho - \rho_l}. \tag{28}$$

Because in (28), $\ln \rho + 1$ represents the slope of the tangent line to the curve p at the point ρ, and $\frac{\rho \ln \rho - \rho_l \ln \rho_l}{\rho - \rho_l}$ represents the slope of the secant line to the curve p passing through points ρ and ρ_l, we next analyze the monotonicity of $G(\rho)$ by using the property of p. Now, we discuss three cases for the initial data.

Case 1. If $0 < \rho_l < \frac{1}{e}$, we know that $\rho_r \geq \rho_l^* > \rho_l$ and

$$\frac{\rho_r \ln \rho_r - \rho_l \ln \rho_l}{\rho_r - \rho_l} \geq 0, \tag{29}$$

which means $P_0 \geq \rho_l^* > \rho_l$ by (26). See Figure 4a. In Figure 4, the solid lines denote the secant lines which connect the left state ρ_l and the right state ρ_r. The dashed lines denote the tangent line at the right state ρ_r.

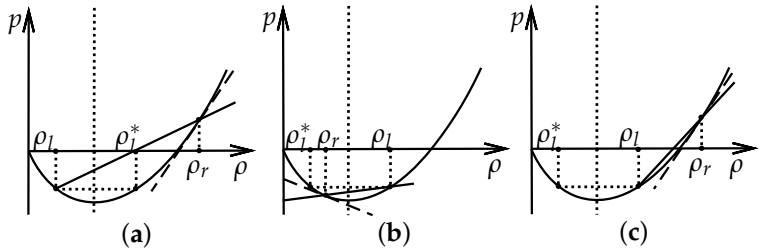

Figure 4. The three cases for the initial data in different regions. (**a**) $0 < \rho_l < \frac{1}{e}, \rho_r > \rho_l^*$. (**b**) $\rho_l > \frac{1}{e}, \rho_r < \rho_l$. (**c**) $\rho_l > \frac{1}{e}, \rho_r > \rho_l$.

For all $\rho > \rho_l^*$, we have

$$\ln \rho + 1 > \frac{\rho \ln \rho - \rho_l \ln \rho_l}{\rho - \rho_l}, \tag{30}$$

where the left side is the slope of the tangent line at ρ, and the right side is the slope of the secant line from ρ_l to ρ. Then, it holds that $G'(\rho) > 0$. Thus, (26) holds if and only if $P_0 = \rho_r$, which contradicts that P_0 is different from ρ_r.

Case 2. If $\rho_l \geq \frac{1}{e}$, we know that $\rho_r \geq \rho_l^*$ and (29) holds, which means $P_0 \geq \rho_l^*$ by (26). In this case, $\rho_l^* \leq P_0 < \rho_l$, then for any $\rho_l^* \leq \rho < \rho_l$, it holds that

$$\ln \rho + 1 < \frac{\rho \ln \rho - \rho_l \ln \rho_l}{\rho - \rho_l}, \tag{31}$$

which means that $G'(\rho) > 0$. See Figure 4b.

Case 3. If $\rho_l \geq \frac{1}{e}$ and $\rho_r > \rho_l$, which means $P_0 > \rho_l$, then (30) holds, which also means that $G'(\rho) > 0$. See Figure 4c.

In conclusion, (26) holds if and only if $P_0 = \rho_r$, which contradicts that P_0 is different from ρ_r. We know that $P(\zeta)$ is strictly monotonous from $-\infty$ to $+\infty$. □

According to Lemma 1, if $P > \rho_l$, then it holds that $P'(\zeta) > 0$. If $P < \rho_l$, it holds that $P'(\zeta) < 0$. Thus, we have that $\frac{P'(\zeta)}{P-\rho_l} > 0$. For any P between ρ_l and ρ_r, it holds that $\frac{M-m_l}{P-\rho_l} - \frac{P'(\zeta)}{P-\rho_l} < \frac{M-m_l}{P-\rho_l}$. From the first equality of (22), we have that

$$s = \frac{m_r - m_l}{\rho_r - \rho_l} < \frac{m - m_l}{\rho - \rho_l}, \quad \text{as} \quad \varepsilon \to 0^+ \tag{32}$$

for any ρ between ρ_l and ρ_r. As the viscosity admissibility criterion for a discontinuity, (32) is called the entropy condition.

3.3. Admissible Shock Waves

In this subsection, we pick up the unique admissible shock waves by the entropy condition (32) from the Hugoniot curves (16) and analyze the properties of them. Assume that the left state is (ρ_l, m_l) and the right state is (ρ, m). To solve the Riemann problem of (1) by a single shock wave, we categorize the initial data into four distinct cases, as follows:

I, $\rho > \rho_l \geq \frac{1}{e}$; II, $\rho > \frac{1}{e} > \rho_l$; III, $\rho_l > \rho \geq \frac{1}{e}$; IV, $\rho_l > \frac{1}{e} > \rho$. Next, we analyze the shock waves case by case.

Case I. $\rho > \rho_l \geq \frac{1}{e}$. It means that the initial data are in the hyperbolic region. To obtain the admissible shock wave, we pick it from the discontinuity curves (17) satisfying (32).

If the shock wave satisfies

$$\frac{m - m_l}{\rho - \rho_l} = \frac{m_l}{\rho_l} - \sqrt{\frac{\rho(\rho \ln \rho - \rho_l \ln \rho_l)}{\rho_l(\rho - \rho_l)}}, \tag{33}$$

we have that

$$\begin{cases} \frac{m_r - m_l}{\rho_r - \rho_l} & = \frac{m_l}{\rho_l} - \sqrt{\frac{\rho_r(\rho_r \ln \rho_r - \rho_l \ln \rho_l)}{\rho_l(\rho_r - \rho_l)}}, \\ \frac{m - m_l}{\rho - \rho_l} & = \frac{m_l}{\rho_l} - \sqrt{\frac{\rho(\rho \ln \rho - \rho_l \ln \rho_l)}{\rho_l(\rho - \rho_l)}}, \end{cases} \tag{34}$$

where the state (ρ, m) satisfies $\rho_l < \rho < \rho_r$. It holds that $G'(\rho) > 0$ where $G(\rho)$ satisfies (27).

Thus, it holds that

$$\frac{\rho_r(\rho_r \ln \rho_r - \rho_l \ln \rho_l)}{\rho_r - \rho_l} > \frac{\rho(\rho \ln \rho - \rho_l \ln \rho_l)}{\rho - \rho_l}, \tag{35}$$

which means the shock wave satisfies the entropy condition (32). In addition, according to $\rho > \rho_l > \frac{1}{e}$ and

$$\ln \rho_l + 1 < \frac{\rho \ln \rho - \rho_l \ln \rho_l}{\rho - \rho_l} < \ln \rho + 1,$$

we know that the speed of the shock wave satisfies

$$s = \frac{m - m_l}{\rho - \rho_l} = u_l - \sqrt{\frac{\rho(\rho \ln \rho - \rho_l \ln \rho_l)}{\rho_l(\rho - \rho_l)}} < u_l - \sqrt{\ln \rho_l + 1} = \lambda_1(\rho_l, u_l). \tag{36}$$

And it holds that

$$s = \frac{m - m_l}{\rho - \rho_l} = u - \sqrt{\frac{\rho_l(\rho \ln \rho - \rho_l \ln \rho_l)}{\rho(\rho - \rho_l)}} > u - \sqrt{\ln \rho + 1} = \lambda_1(\rho, u). \tag{37}$$

Conditions (36) and (37) are the Lax entropy conditions for 1-shock waves.

If the shock wave satisfies

$$\frac{m - m_l}{\rho - \rho_l} = \frac{m_l}{\rho_l} + \sqrt{\frac{\rho(\rho \ln \rho - \rho_l \ln \rho_l)}{\rho_l(\rho - \rho_l)}}, \tag{38}$$

we have that

$$\begin{cases} \frac{m_r - m_l}{\rho_r - \rho_l} & = \frac{m_l}{\rho_l} + \sqrt{\frac{\rho_r(\rho_r \ln \rho_r - \rho_l \ln \rho_l)}{\rho_l(\rho_r - \rho_l)}}, \\ \frac{m - m_l}{\rho - \rho_l} & = \frac{m_l}{\rho_l} + \sqrt{\frac{\rho(\rho \ln \rho - \rho_l \ln \rho_l)}{\rho_l(\rho - \rho_l)}}, \end{cases} \tag{39}$$

where the state (ρ, m) satisfies $\rho_l < \rho < \rho_r$. Taking it into (32), it holds that

$$\frac{\rho_r(\rho_r \ln \rho_r - \rho_l \ln \rho_l)}{\rho_r - \rho_l} < \frac{\rho(\rho \ln \rho - \rho_l \ln \rho_l)}{\rho - \rho_l}. \tag{40}$$

It contradicts with (35) for $\rho_r > \rho > \rho_l > \frac{1}{e}$. Thus, (38) is not an admissible shock wave.

Based on the above analysis, we obtain the 1-shock wave denoted by S_1, which satisfies

$$S_1(\rho_l, m_l): \begin{cases} \dfrac{m-m_l}{\rho-\rho_l} = \dfrac{m_l}{\rho_l} - \sqrt{\dfrac{\rho(\rho\ln\rho - \rho_l\ln\rho_l)}{\rho_l(\rho-\rho_l)}}, & \rho > \rho_l \geq \dfrac{1}{\mathrm{e}}, \\ \lambda_1(\rho,u) < s < \lambda_1(\rho_l,u_l). \end{cases} \tag{41}$$

In addition, along the shock wave S_1, we have that

$$\frac{\mathrm{d}}{\mathrm{d}\rho}\left(\frac{m-m_l}{\rho-\rho_l}\right) = -\frac{G'(\rho)}{2\sqrt{\rho_l G(\rho)}} < 0, \tag{42}$$

where $G(\rho)$ is defined by (27). Now, we depict the 1-shock wave $S_1(\rho_l, m_l)$ for the left state (ρ_l, m_l) in the hyperbolic region H_1 with a solid curve, as shown in Figure 5. Hereafter, we mark Ⓛ as the left state (ρ_l, m_l) shown in Figure 5. The dotted curves denote the shock waves $S_1(\rho_l, m_l)$ from the left state (ρ_l, m_l), which is in hyperbolic region H_2 or H_3.

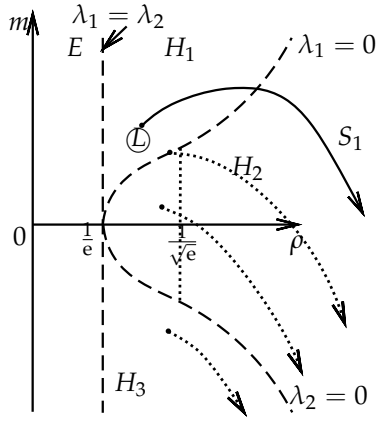

Figure 5. The first family shock wave $S_1(\rho_l, m_l)$ if the left state (ρ_l, m_l) is in the hyperbolic region.

Remark 1. *For this case, if the left state is in the region of H_1 (see Figure 5), there is a stationary shock wave such that $\frac{\mathrm{d}x}{\mathrm{d}t} = 0$, that is, $m = m_l$ and $\frac{m^2}{\rho} + \rho\ln\rho = \frac{m_l^2}{\rho_l} + \rho_l\ln\rho_l$.*

Case II. $\rho > \frac{1}{\mathrm{e}} > \rho_l$. It means that the left state (ρ_l, u_l) is in the elliptical region and the right state (ρ, u) is in the hyperbolic region. There exists a unique $\rho_l^* > \frac{1}{\mathrm{e}}$ such that $\rho_l^*\ln\rho_l^* = \rho_l\ln\rho_l$. If the discontinuity curve exists, it must hold that $\rho \geq \rho_l^* > \frac{1}{\mathrm{e}} > \rho_l$. For this case, the shock wave which should satisfy (17) is no longer a continuity curve. And there is a jump from the left state to the right state. Similar to Case I, according to the entropy condition (32), we obtain the 1-shock wave denoted by S_1^E (see Figure 6) satisfying

$$S_1^E(\rho_l, m_l): \begin{cases} \dfrac{m-m_l}{\rho-\rho_l} = \dfrac{m_l}{\rho_l} - \sqrt{\dfrac{\rho(\rho\ln\rho - \rho_l\ln\rho_l)}{\rho_l(\rho-\rho_l)}}, \rho \geq \rho_l^* > \dfrac{1}{\mathrm{e}} > \rho_l, \\ \lambda_1(\rho,u) < s \leq u_l. \end{cases} \tag{43}$$

In Figure 6, the dotted curves denote the S_1^E from (ρ_l^*, m_l^*) where the left state with the same ρ_l and the different m_l is in the elliptic region. Along this shock wave S_1^E, we have that

$$\frac{\mathrm{d}}{\mathrm{d}\rho}\left(\frac{m-m_l}{\rho-\rho_l}\right) = -\frac{G'(\rho)}{2\sqrt{\rho_l G(\rho)}} < 0. \tag{44}$$

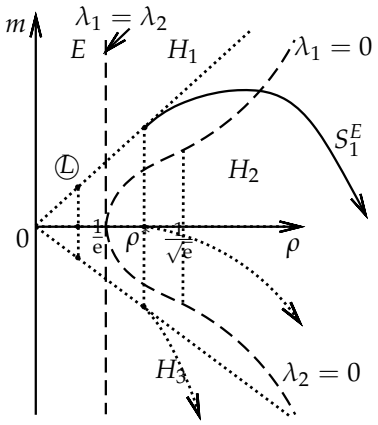

Figure 6. The first family shock wave S_1^E if the left state (ρ_l, m_l) is in the elliptic region.

Case III. $\rho_l > \rho \geq \frac{1}{e}$. It means that both left and right states are in the hyperbolic region. Then, by the entropy condition (32), we obtain the 2-shock wave denoted by S_2 (see Figure 7), which satisfies

$$S_2(\rho_l, m_l): \begin{cases} \dfrac{m - m_l}{\rho - \rho_l} = \dfrac{m_l}{\rho_l} + \sqrt{\dfrac{\rho(\rho \ln \rho - \rho_l \ln \rho_l)}{\rho_l(\rho - \rho_l)}}, \rho_l > \rho \geq \dfrac{1}{e}, \\ \lambda_2(\rho, u) < s < \lambda_2(\rho_l, u_l). \end{cases} \tag{45}$$

The dotted curves denote the S_2 from the left state (ρ_l, m_l) in a different hyperbolic region. Along this shock wave S_2, we have that

$$\frac{\mathrm{d}}{\mathrm{d}\rho}\left(\frac{m - m_l}{\rho - \rho_l}\right) = \frac{G'(\rho)}{2\sqrt{\rho_l G(\rho)}} > 0. \tag{46}$$

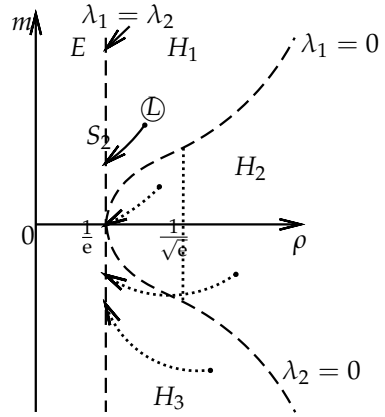

Figure 7. The second family shock wave S_2 if both the left state (ρ_l, m_l) and the right state are in the hyperbolic region.

Case IV. $\rho_l > \frac{1}{e} > \rho$. It means that the left state (ρ_l, u_l) is in the hyperbolic region and the right state (ρ, u) is in the elliptical region. There are two subcases.

Subcase IV.1. If $\frac{1}{e} < \rho_l \leq 1$, there exists a unique $\rho_l^* < \frac{1}{e}$ such that $\rho_l^* \ln \rho_l^* = \rho_l \ln \rho_l$. If the discontinuity curve exists, it must hold that $\rho_l > \frac{1}{e} > \rho > \rho_l^*$. Then, according to the entropy condition (32), we obtain the 2-shock wave denoted by S_2^E (see Figure 8) satisfying

$$S_2^E(\rho_l, m_l): \begin{cases} \dfrac{m - m_l}{\rho - \rho_l} = \dfrac{m_l}{\rho_l} + \sqrt{\dfrac{\rho(\rho \ln \rho - \rho_l \ln \rho_l)}{\rho_l(\rho - \rho_l)}}, \rho_l > \dfrac{1}{e} > \rho > \rho_l^*, \\ u \leq s < \lambda_2(\rho_l, u_l). \end{cases} \tag{47}$$

In Figure 8, the dotted curves denote the S_2^E from the boundary of the elliptic region to the (ρ_l^*, m_l^*), where the left state (ρ_l, m_l) is in a different hyperbolic region with the same ρ_l and different m_l. Along this shock wave S_2^E, we have that

$$\frac{\mathrm{d}}{\mathrm{d}\rho}\left(\frac{m - m_l}{\rho - \rho_l}\right) = \frac{G'(\rho)}{2\sqrt{\rho_l G(\rho)}} > 0. \tag{48}$$

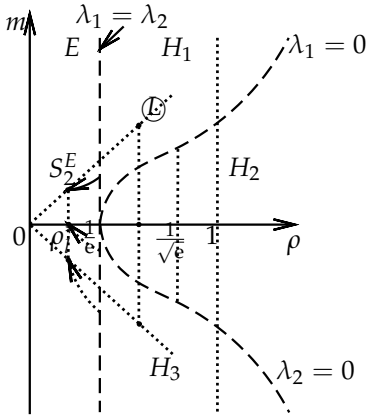

Figure 8. The second family shock wave S_2^E for the left state (ρ_l, m_l) in the hyperbolic region and the right state in the elliptic region.

Subcase IV.2. If $\rho_l > 1$, the 2-shock wave denoted by $S_2^{\bar{E}}$ (see Figure 9) satisfies

$$S_2^{\bar{E}}(\rho_l, m_l): \begin{cases} \dfrac{m - m_l}{\rho - \rho_l} = \dfrac{m_l}{\rho_l} + \sqrt{\dfrac{\rho(\rho \ln \rho - \rho_l \ln \rho_l)}{\rho_l(\rho - \rho_l)}}, \rho_l > 1 > \dfrac{1}{e} > \rho > 0, \\ u < s < \lambda_2(\rho_l, u_l). \end{cases} \tag{49}$$

In Figure 9, the dotted curves denote the $S_2^{\bar{E}}$ from the left state (ρ_l, u_l) in the different hyperbolic region to the original point. Along this shock wave $S_2^{\bar{E}}$, we have that

$$\frac{\mathrm{d}}{\mathrm{d}\rho}\left(\frac{m - m_l}{\rho - \rho_l}\right) = \frac{G'(\rho)}{2\sqrt{\rho_l G(\rho)}} > 0. \tag{50}$$

Based on the above analysis, we know that for Case I, the wave is the first family shock wave which is in the hyperbolic region. For Case II, the wave is also the first family shock wave, while it is not connected. For case III, the wave is the second family shock wave which is in the hyperbolic region. For case IV, the wave is the second family shock wave, while it is not connected. In fact, for case III and case IV, the two shock waves form a continuity curve for the same left state.

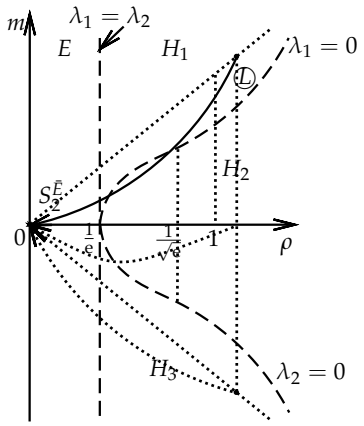

Figure 9. The second family shock wave $S_2^{\bar{E}}$ if the left state (ρ_l, m_l) is in the hyperbolic region, while the right state can be in the hyperbolic region or in the elliptic region.

Remark 2. *We illustrate that the notations S, S^E, and $S^{\bar{E}}$ all denote the shock waves. But there is a little difference. If both the left state and right state are in the hyperbolic region, the shock wave is marked S. If one of the two states is in the hyperbolic region and the other one is in the elliptic region, the shock wave is marked S^E. If one of the states is in the hyperbolic region and the other state can be in both regions, the shock wave is marked $S^{\bar{E}}$. For example, for Case III, the shock wave is S_2. For Case IV, the shock wave is S_2^E. Then, it holds that $S_2^{\bar{E}} = S_2 \cup S_2^E$.*

4. Rarefaction Waves

A rarefaction wave is a continuous solution of (1) of form $(\rho, u)(\xi)$, $\xi = \frac{x}{t}$. The k-rarefaction wave curves are the sets of states that are connected to (ρ_l, m_l), which means that the k-Riemann invariants ω_k are constants, $k = 1, 2$. Then, we obtain the equations of the 1-rarefaction wave denoted by R_1 and 2-rarefaction wave denoted by R_2 (see Figure 10). In Figure 10, the dotted curves denote R_1 from (ρ_l, m_l) to the boundary of the elliptic region and R_2 from (ρ_l, m_l) to infinity.

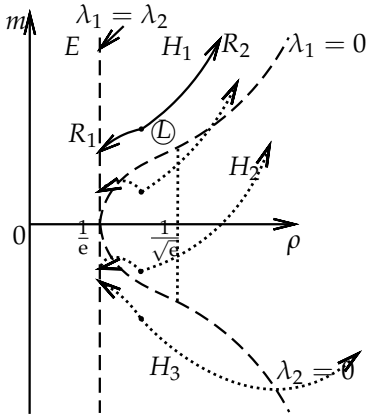

Figure 10. The rarefaction waves R_1 and R_2 if the left state (ρ_l, m_l) is in the hyperbolic region H.

The 1-rarefaction wave R_1 satisfies

$$R_1(\rho_l, m_l): \begin{cases} m - m_l = \frac{m_l}{\rho_l}(\rho - \rho_l) - \frac{2}{3}\rho\Big((\ln\rho + 1)^{\frac{3}{2}} - (\ln\rho_l + 1)^{\frac{3}{2}}\Big), & \rho_l > \rho > \frac{1}{e}, \\ \xi = u - \sqrt{\ln\rho + 1}. \end{cases} \tag{51}$$

Along the R_1, we have that

$$\begin{cases} \frac{\mathrm{d}m}{\mathrm{d}\rho} = \frac{m_l}{\rho_l} - \frac{2}{3}\Big((\ln\rho+1)^{\frac{3}{2}} - (\ln\rho_l+1)^{\frac{3}{2}}\Big) - \sqrt{\ln\rho+1} = \lambda_1(\rho,u), \\ \frac{\mathrm{d}^2m}{\mathrm{d}\rho^2} = -\frac{\sqrt{\ln\rho+1}}{\rho} - \frac{1}{2\rho\sqrt{\ln\rho+1}} < 0. \end{cases} \tag{52}$$

The 2-rarefaction wave R_2 satisfies

$$R_2(\rho_l, m_l): \begin{cases} m - m_l = \frac{m_l}{\rho_l}(\rho-\rho_l) + \frac{2}{3}\rho\Big((\ln\rho+1)^{\frac{3}{2}} - (\ln\rho_l+1)^{\frac{3}{2}}\Big), \quad \rho > \rho_l > \frac{1}{\mathrm{e}}, \\ \xi = u + \sqrt{\ln\rho+1}. \end{cases} \tag{53}$$

Along the R_2, we have that

$$\begin{cases} \frac{\mathrm{d}m}{\mathrm{d}\rho} = \frac{m_l}{\rho_l} + \frac{2}{3}\Big((\ln\rho+1)^{\frac{3}{2}} - (\ln\rho_l+1)^{\frac{3}{2}}\Big) + \sqrt{\ln\rho+1} = \lambda_2(\rho,u), \\ \frac{\mathrm{d}^2m}{\mathrm{d}\rho^2} = \frac{\sqrt{\ln\rho+1}}{\rho} + \frac{1}{2\rho\sqrt{\ln\rho+1}} > 0. \end{cases} \tag{54}$$

5. Riemann Solutions

In this section, we construct the Riemann solution for the mixed-type model (1) and (2) with the initial data (5). For the fixed left state (ρ_l, m_l), we divide the (ρ, m) plane into several regions by the shock waves in Section 3 and the rarefaction waves in Section 4. In the following, we will analyze two cases, where the left states are in the elliptic region $(0 < \rho_l < \frac{1}{\mathrm{e}})$ and hyperbolic region $(\rho_l \geq \frac{1}{\mathrm{e}})$, respectively.

Case 1. Assuming that (ρ_l, u_l) is in the elliptic region, that is, $0 < \rho_l < \frac{1}{\mathrm{e}}$, we construct the Riemann solutions for the right state in the solvable regions I and II, as in Figure 11. The boundaries of region I are $R_2(\rho_l^*, m_l^*)$ and $S_1^E(\rho_l, m_l)$ with $\rho > \rho_l^*$. The boundaries of region II are $S_1^E(\rho_l, m_l)$, $S_2(\rho_l^*, m_l^*)$, $S_2^E(\rho_l^*, m_l^*)$, Γ and the negative axis of m, where Γ satisfies

$$\begin{aligned} \{(\rho,m)|m = &\frac{m^*}{\rho^*}\rho, m^* = \frac{m_l}{\rho_l}\rho^* - (\rho^*-\rho_l)\sqrt{\frac{\rho^*(\rho^*\ln\rho^* - \rho_l\ln\rho_l)}{\rho_l(\rho^*-\rho_l)}}, \rho_l^* < \rho^* < 1, \\ &\rho\ln\rho = \rho^*\ln\rho^*, 0 < \rho < \rho_l\}. \end{aligned} \tag{55}$$

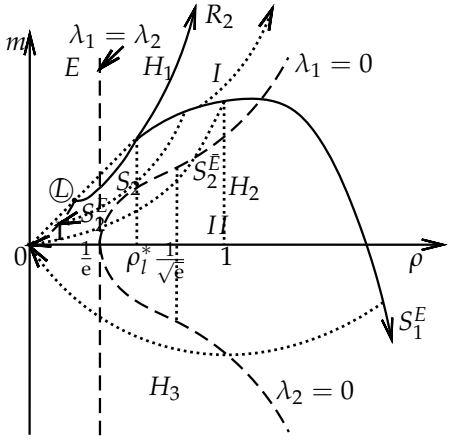

Figure 11. The left state (ρ_l, m_l) is in the elliptic region and the right state is in region I or II.

If the right states (ρ_r, m_r) are located in the region of I, then the solution is constructed as

$$(\rho_l, m_l) \xrightarrow{S_1^E} (\rho_1, m_1) \xrightarrow{R_2} (\rho_r, m_r), \tag{56}$$

where (ρ_1, m_1) satisfy

$$\begin{cases} \frac{m_1-m_l}{\rho_1-\rho_l} = \frac{m_l}{\rho_l} - \sqrt{\frac{\rho_1(\rho_1\ln\rho_1-\rho_l\ln\rho_l)}{\rho_l(\rho_1-\rho_l)}}, \\ m_r - m_1 = \frac{m_1}{\rho_1}(\rho_r-\rho_1) + \frac{2}{3}\rho_r\Big((\ln\rho_r+1)^{\frac{3}{2}} - (\ln\rho_1+1)^{\frac{3}{2}}\Big). \end{cases} \tag{57}$$

If the right states (ρ_r, m_r) are located in the region of II, then the solution is constructed as

$$(\rho_l, m_l) \xrightarrow{S_1^E} (\rho_1, m_1) \xrightarrow{S_2 \text{ or } S_2^E \text{ or } S_2^{\tilde{E}}} (\rho_r, m_r), \tag{58}$$

where (ρ_1, m_1) satisfy

$$\begin{cases} \frac{m_1-m_l}{\rho_1-\rho_l} = \frac{m_l}{\rho_l} - \sqrt{\frac{\rho_1(\rho_1\ln\rho_1-\rho_l\ln\rho_l)}{\rho_l(\rho_1-\rho_l)}}, \\ \frac{m_r-m_1}{\rho_r-\rho_1} = \frac{m_1}{\rho_1} + \sqrt{\frac{\rho_r(\rho_r\ln\rho_r-\rho_1\ln\rho_1)}{\rho_1(\rho_r-\rho_1)}}. \end{cases} \tag{59}$$

Case 2. Assuming that the (ρ_l, u_l) is in the hyperbolic region of $H_1 = \{(\rho, m)|\rho > \frac{1}{\mathrm{e}}, 0 < \lambda_1 < \lambda_2\}$, we construct the Riemann solutions for the right state in different regions. There are two subcases.

Subcase 2.1. $\frac{1}{\mathrm{e}} \le \rho_l \le 1$. We construct the Riemann solutions for the right state in the solvable regions I', II', III', and IV', as in Figure 12. The boundaries of I' are $R_2(\rho_l, m_l)$ and $S_1(\rho_l, m_l)$ with $\rho > \rho_l$. The boundaries of II' are $R_1(\rho_l, m_l)$, $R_2(\rho_l, m_l)$, and $R_2(\frac{1}{\mathrm{e}}, m_e)$, where $(\frac{1}{\mathrm{e}}, m_e)$ is on the curve $R_1(\rho_l, m_l)$. The boundaries of III' are $R_1(\rho_l, m_l)$, $S_2(\rho_l, m_l)$, $S_2^E(\rho_l, m_l)$ and Γ_1, where Γ_1 satisfies

$$\begin{aligned} \{(\rho, m)|m = \frac{m^*}{\rho^*}\rho, m^* = \frac{m_l}{\rho_l}\rho^* - \frac{2}{3}\rho^*\Big((\ln\rho^*+1)^{\frac{3}{2}} - (\ln\rho_l+1)^{\frac{3}{2}}\Big), \frac{1}{\mathrm{e}} < \rho^* < \rho_l, \\ \rho\ln\rho = \rho^*\ln\rho^*\}. \end{aligned} \tag{60}$$

The boundaries of IV' are $S_1(\rho_l, m_l)$, $S_2(\rho_l, m_l)$, $S_2^E(\rho_l, m_l)$, Γ_2 and the negative axis of m, where Γ_2 satisfies

$$\begin{aligned} \{(\rho, m)|m = &\frac{m^*}{\rho^*}\rho, m^* = \frac{m_l}{\rho_l}\rho^* - (\rho^*-\rho_l)\sqrt{\frac{\rho^*(\rho^*\ln\rho^*-\rho_l\ln\rho_l)}{\rho_l(\rho^*-\rho_l)}}, \\ &\rho\ln\rho = \rho^*\ln\rho^*, 0 < \rho < \rho_l^*\}. \end{aligned} \tag{61}$$

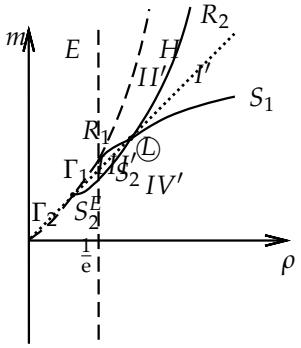

Figure 12. The left state (ρ_l, m_l) is in the hyperbolic region for $\frac{1}{\mathrm{e}} \le \rho_l \le 1$, and the right state is in region I', II', III', or IV'.

If the right states (ρ_r, m_r) are located in the region of I', then the solution is constructed as

$$(\rho_l, m_l) \xrightarrow{S_1} (\rho_1, m_1) \xrightarrow{R_2} (\rho_r, m_r), \tag{62}$$

where (ρ_1, m_1) satisfy

$$\begin{cases} \frac{m_1-m_l}{\rho_1-\rho_l} = \frac{m_l}{\rho_l} - \sqrt{\frac{\rho_1(\rho_1\ln\rho_1-\rho_l\ln\rho_l)}{\rho_l(\rho_1-\rho_l)}}, \\ m_r - m_1 = \frac{m_1}{\rho_1}(\rho_r-\rho_1) + \frac{2}{3}\rho_r\Big((\ln\rho_r+1)^{\frac{3}{2}} - (\ln\rho_1+1)^{\frac{3}{2}}\Big). \end{cases} \tag{63}$$

If the right states (ρ_r, m_r) are located in the region of II', then the solution is constructed as

$$(\rho_l, m_l) \xrightarrow{R_1} (\rho_1, m_1) \xrightarrow{R_2} (\rho_r, m_r), \tag{64}$$

where (ρ_1, m_1) satisfy

$$\begin{cases} m_1 - m_l = \frac{m_l}{\rho_l}(\rho_1-\rho_l) - \frac{2}{3}\rho_1\Big((\ln\rho_1+1)^{\frac{3}{2}} - (\ln\rho_l+1)^{\frac{3}{2}}\Big), \\ m_r - m_1 = \frac{m_1}{\rho_1}(\rho_r-\rho_1) + \frac{2}{3}\rho_r\Big((\ln\rho_r+1)^{\frac{3}{2}} - (\ln\rho_1+1)^{\frac{3}{2}}\Big). \end{cases} \tag{65}$$

Similar to case 1, the solution may also be constructed as

$$(\rho_l, m_l) \xrightarrow{S_2} (\rho_1, m_1) \xrightarrow{R_2} (\rho_r, m_r). \tag{66}$$

If the right states (ρ_r, m_r) are located in the region of III', then the solution is constructed as

$$(\rho_l, m_l) \xrightarrow{R_1} (\rho_1, m_1) \xrightarrow{S_2 \text{ or } S_2^E} (\rho_r, m_r), \tag{67}$$

where (ρ_1, m_1) satisfy

$$\begin{cases} m_1 - m_l = \frac{m_l}{\rho_l}(\rho_1-\rho_l) - \frac{2}{3}\rho_1\Big((\ln\rho_1+1)^{\frac{3}{2}} - (\ln\rho_l+1)^{\frac{3}{2}}\Big), \\ \frac{m_r-m_1}{\rho_r-\rho_1} = \frac{m_1}{\rho_1} + \sqrt{\frac{\rho_r(\rho_r\ln\rho_r-\rho_1\ln\rho_1)}{\rho_1(\rho_r-\rho_1)}}. \end{cases} \tag{68}$$

If the right states (ρ_r, m_r) are located in the region of IV', then the solution is constructed as

$$(\rho_l, m_l) \xrightarrow{S_1} (\rho_1, m_1) \xrightarrow{S_2 \text{ or } S_2^E} (\rho_r, m_r), \tag{69}$$

where (ρ_1, m_1) satisfy

$$\begin{cases} \frac{m_1-m_l}{\rho_1-\rho_l} = \frac{m_l}{\rho_l} - \sqrt{\frac{\rho_1(\rho_1\ln\rho_1-\rho_l\ln\rho_l)}{\rho_l(\rho_1-\rho_l)}}, \\ \frac{m_r-m_1}{\rho_r-\rho_1} = \frac{m_1}{\rho_1} + \sqrt{\frac{\rho_r(\rho_r\ln\rho_r-\rho_1\ln\rho_1)}{\rho_1(\rho_r-\rho_1)}}. \end{cases} \tag{70}$$

Subcase 2.2. $\rho_l \geq 1$. We construct the Riemann solutions for the right state in the solvable regions I'', II'', III'', and IV'', as in Figure 13. The boundaries of I'' are $R_2(\rho_l, m_l)$ and $S_1(\rho_l, m_l)$ with $\rho > \rho_l$. The boundaries of II'' are $R_1(\rho_l, m_l)$, $R_2(\rho_l, m_l)$, and $R_2(\frac{1}{\mathrm{e}}, m_e)$, where $(\frac{1}{\mathrm{e}}, m_e)$ is on the curve $R_1(\rho_l, m_l)$. The boundaries of III'' are $R_1(\rho_l, m_l)$, $S_2^{\bar{E}}(\rho_l, m_l)$, and $\bar{\Gamma}$, where $\bar{\Gamma}$ satisfies

$$\begin{aligned} \{(\rho, m) | m = \frac{m^*}{\rho^*}\rho, m^* = \frac{m_l}{\rho_l}\rho^* - \frac{2}{3}\rho^*\Big((\ln\rho^*+1)^{\frac{3}{2}} - (\ln\rho_l+1)^{\frac{3}{2}}\Big), \\ \rho\ln\rho = \rho^*\ln\rho^*, \frac{1}{\mathrm{e}} < \rho^* < 1\}. \end{aligned} \tag{71}$$

The boundaries of IV'' are $S_2^{\bar{E}}(\rho_l, m_l)$ and $S_1(\rho_l, m_l)$.

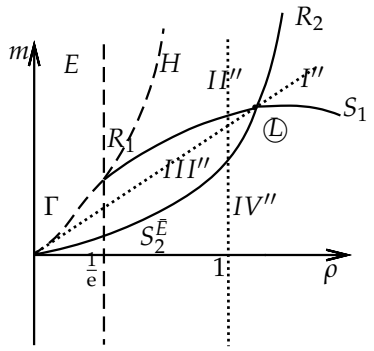

Figure 13. The left state (ρ_l, m_l) is in the hyperbolic region for $\rho_l \geq 1$, and the right state is in region I'', II'', III'', or IV''.

If the right states (ρ_r, m_r) are located in the region of I'', then the solution is constructed as (62). If the right states (ρ_r, m_r) are located in the region of II'', then the solution is constructed as (64). If the right states (ρ_r, m_r) are located in the region of III'', then the solution is constructed as (67). If the right states (ρ_r, m_r) are located in the region of IV'', then the solution is constructed as

$$(\rho_l, m_l) \xrightarrow{S_1} (\rho_1, m_1) \xrightarrow{S_2^{\bar{E}}} (\rho_r, m_r), \tag{72}$$

where (ρ_1, m_1) satisfy

$$\begin{cases} \frac{m_1 - m_l}{\rho_1 - \rho_l} = \frac{m_l}{\rho_l} - \sqrt{\frac{\rho_1(\rho_1 \ln \rho_1 - \rho_l \ln \rho_l)}{\rho_l(\rho_1 - \rho_l)}}, \\ \frac{m_r - m_1}{\rho_r - \rho_1} = \frac{m_1}{\rho_1} + \sqrt{\frac{\rho_r(\rho_r \ln \rho_r - \rho_1 \ln \rho_1)}{\rho_1(\rho_r - \rho_1)}}. \end{cases} \tag{73}$$

Similarly, if the left state is in the hyperbolic region of H_2 or H_3 with $\rho_l > 1$, the unique Riemann solution can be also constructed. We omit them. In conclusion, we have the following result.

Theorem 1. *For the fixed left states (ρ_l, u_l) and the right states (ρ_r, u_r) in the feasible regions as described in cases 1 and 2 (see Figures 11–13), the Riemann problems (1), (2), and (5) have a unique weak solution satisfying the entropy condition (32).*

6. Numerical Tests

In this section, we present some numerical tests to verify our theoretical results for the construction of the Riemann solutions for (1) and (2) with initial data (5). We use the essentially non-oscillatory (ENO) scheme [40] and third-order Runge–Kutta method with 60×60 cells. The $CFL = 0.4$ and the running time $T = 0.2$. Many more numerical tests have been performed to make sure that what are presented are not numerical artifacts. Here, we present three cases to verify our theoretical solution.

Case 1. In this case, we take the initial Riemann data as

$$(\rho, u)|_{t=0} = \begin{cases} (1.2, 1) & x < 0, \\ (0.2, 1) & x > 0, \end{cases} \tag{74}$$

where the left state $(1.2, 1)$ belongs to the hyperbolic region and the right state $(0.2, 1)$ belongs to the elliptic region.

As marked in Figures 14–16, the red and blue lines in the upper half plane represent approximate density and velocity, and the yellow and green lines in the lower half plane represent the exact density and velocity, respectively. From Figure 14, we find that the left state of (74) is connected to the intermediate state by a rarefaction wave, and then to the

right state of (74) by a shock wave. This verifies the theoretical solution for Subcase 2.2 in Section 5 in which the right state is located in region III'' of the left state.

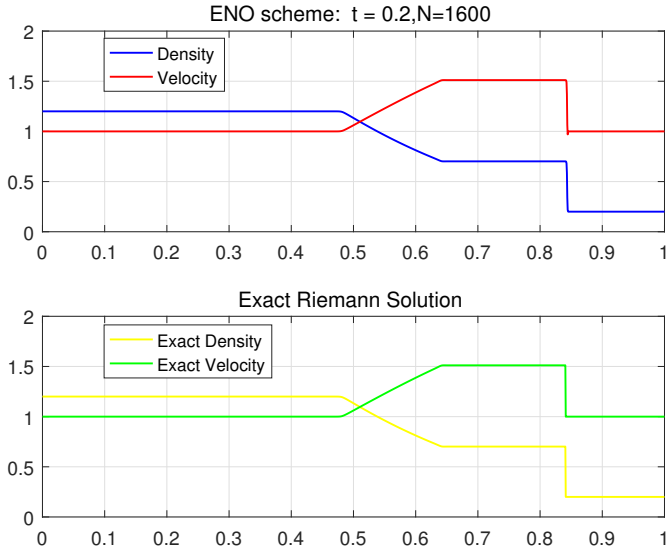

Figure 14. Riemann solution for (1), (2), and (74). The left state is in the hyperbolic region, and the right state is in the elliptic region.

Case 2. In this case, we take the initial Riemann data as

$$(\rho, u)|_{t=0} = \begin{cases} (0.2, 1) & x < 0, \\ (0.8, 0.1) & x > 0, \end{cases} \tag{75}$$

where the left state $(0.2, 1)$ belongs to the elliptic region and the right state $(0.8, 0.1)$ belongs to the hyperbolic region. From Figure 15, the Riemann solution consists of three constant states separated by two shock waves. Specifically, the left state of (75) is connected to the intermediate state by a shock wave, and then to the right state of (75) by a shock wave. This verifies the theoretical solution for Case 1 in Section 5 in which the right state is located in region II of the left state.

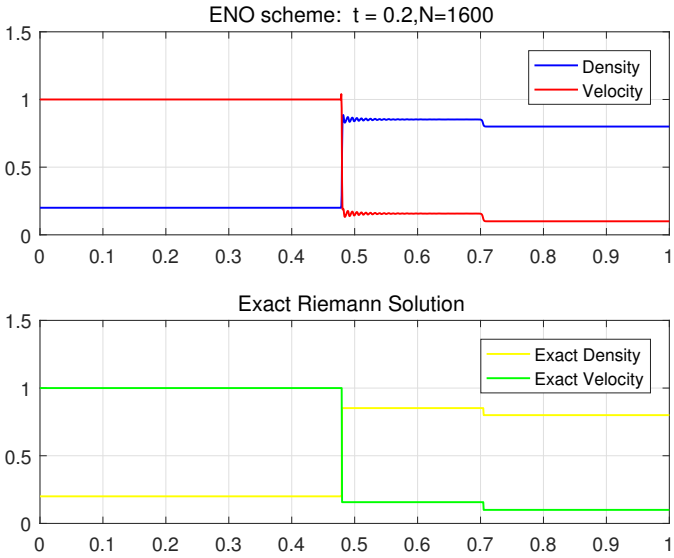

Figure 15. Riemann solution for (1), (2), and (75). The left state is in the elliptic region, and the right state is in the hyperbolic region.

Case 3. In this case, we take the initial Riemann data as

$$(\rho, u)|_{t=0} = \begin{cases} (0.95, 1) & x < 0, \\ (1, 0) & x > 0, \end{cases} \tag{76}$$

where both the left state $(0.95, 1)$ and the right state $(1, 0)$ are in the hyperbolic region. From Figure 16, the Riemann solution also consists of three constant states separated by two shock waves. This verifies the theoretical solution for Subcase 2.1 in Section 5 in which the right state is located in region IV' of the left state.

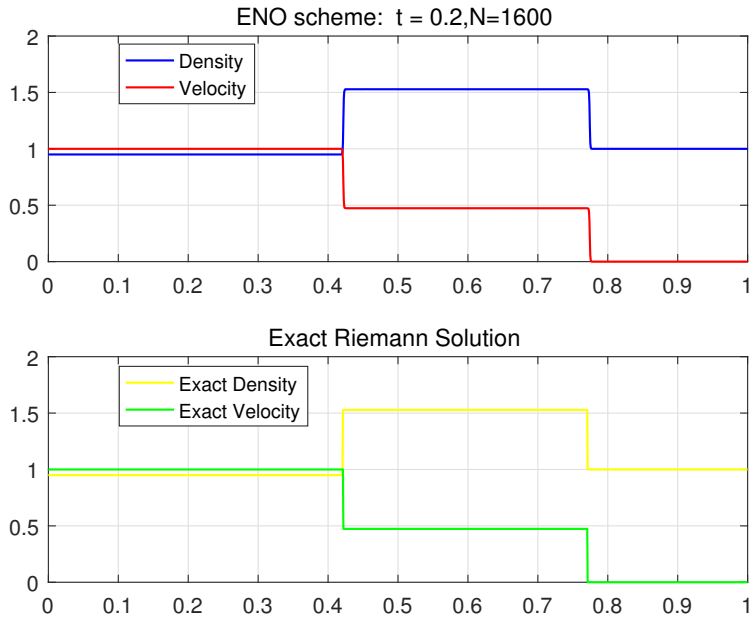

Figure 16. Riemann solution for (1), (2), and (76). Both of the initial states are in the hyperbolic region.

It is worth pointing out that the Gibbs phenomenon [38] appears in Cases 1 and 2, where one of the initial state is in the hyperbolic region, and the other state is in the elliptic region, while in Case 3, where both of the initial states are in the hyperbolic region, the Gibbs phenomenon does not appear. It inspires us to find a better numerical scheme to capture the shock wave in the mixed conservation laws in our further works.

7. Discussion

The shape of the elliptic regions (1) with (2) and the van der Waals models [21] forms a strip. However, for systems (1) and (2), there is one hyperbolic region, while there are two hyperbolic regions for van der Waals, whose nonclassical shocks satisfy a kinetic relation [23]. This difference implies that methods applicable to the study of the van der Waals models are not suitable for systems (1) and (2). Furthermore, in the previous studies [29–31,34], we observe that the challenges in studying mixed-type partial differential equations are contingent upon the shape of the elliptic regions.

From the previous models [29,30,39,41], the uniqueness of the solution of the hyperbolic–elliptic model could not be obtained by the Lax entropy condition or the Liu entropy condition. For our models (1) and (2), the Hugoniot curves (13) are not connected or self-intersecting (see Figure 3). We provide the entropy condition (32) to pick up the admissible shock waves, including the elliptic region.

In this paper, the feasible regions are contained in Figures 11–13. For the ideal gas or Chaplygin gas, the systems are hyperbolic. For these models, a vacuum or a delta shock wave exists in the intractable regions, in which the Riemann solution cannot be constructed by the shock waves and rarefaction waves [15,37]. However, the dark energy

fluid (1) with (2) is of mixed type. The methods for investigating the two systems are different. In our work, there exist intractable regions in each case. This singularity may result in a vacuum, a delta shock wave, or other types of singularities. This problem is worth further study.

8. Conclusions

In this paper, we construct the Riemann solutions for the mixed-type isentropic Euler Equations (1), in which the pressure (2) is a special case of the generalized dark energy EoS (3). Using the Rankine–Hugoniot conditions for the mixed-type systems (1) and (2), we find that the discontinuity curves may exist in both elliptic regions and hyperbolic regions. The classical entropy condition is not applicable. We obtain the unique admissible shock waves by utilizing the viscosity criterion. The principal element in the construction is a division of the (ρ, m)-plane into several regions, the division depending upon the location of (ρ_l, m_l). The solution of the Riemann problem consists of a combination of admissible shock waves and rarefaction waves, the combination determined by the region in which (ρ_r, m_r) lies. Finally, we present numerical simulations which are consistent with our theoretical results.

Author Contributions: Conceptualization, T.C. and W.J.; methodology, T.C., W.J. and J.L.; validation, T.L. and Z.W.; formal analysis, T.C.; investigation, T.L. and Z.W.; resources, W.J.; writing—original draft preparation, T.C.; writing—review and editing, W.J., T.L. and Z.W.; supervision, T.L. and Z.W.; project administration, W.J.; funding acquisition, W.J. and Z.W. All authors have read and agreed to the published version of the manuscript.

Funding: The research of Weifeng Jiang is supported by the Fundamental Research Funds for the Provincial Universities of Zhejiang (Grant No. 2021YW39), the Natural Science Foundation of Zhejiang (Grant No. LQ18A010004), the Subproject of Key Scientific Research Project of Zhejiang Provincial Department of Transportation (Grant No. G92N-1003-21). The research of Zhen Wang is supported by the National Natural Science Foundation of China (Grant No. 11771442).

Data Availability Statement: Data are contained within the article.

Conflicts of Interest: The authors declare no conflicts of interest.

References

1. Diperna, R. Convergence of viscosity method for isentropic gas dynamics. *Commun. Math. Phys.* **1983**, *91*, 1–30. [CrossRef]
2. Oikonomou, V.K. Generalized Logarithmic equation of state in classical and loop quantum cosmology dark energy-dark matter coupled systems. *Ann. Phys.* **2019**, *409*, 167934. [CrossRef]
3. Pan, S.; Yang, W.; Di Valentino, E.; Saridakis, E.N.; Chakraborty, S. Interacting scenarios with dynamical dark energy: Observational constraints and alleviation of the H_0 tension. *Phys. Rev. D* **2019**, *100*, 103520. [CrossRef]
4. Mayer, B.; Anton, H.; Bott, E.; Methfessel, M.; Sticht, J.; Harris, J.; Schmidt, P.C. Ab-initio calculation of the elastic constants and thermal expansion coefficients of Laves phases. *Intermetallics* **2003**, *11*, 23–32. [CrossRef]
5. Chen, G.Q. *The Theory of Compensated Compactness and the System of Isentropic Gas Dynamics*; Math Sciences Research Institute: Berkeley, CA, USA, 1990; Preprint 00527-91.
6. Chen, G.Q.; Le Floch, P. Compressible Euler equations with general pressure law. *Arch. Ration. Mech. Anal.* **2000**, *153*, 221–259. [CrossRef]
7. Chen, G.Q.; Huang, F.M.; Wang, T.Y. Isothermal limit of entropy solutions of the Euler equations for isentropic gas dynamics. *SIAM J. Math. Anal.* **2024**, *56*, 1300–1320. [CrossRef]
8. Ding, X.Q.; Chen, G.Q.; Luo, P.Z. Convergence of the Lax-Friedrichs scheme for isentropic gas dynamics (I). *Acta Math. Sci. (Engl. Ed.)* **1985**, *5*, 415–432. [CrossRef]
9. Ding, X.Q.; Chen, G.Q.; Luo, P.Z. Convergence of the Lax-Friedrichs scheme for isentropic gas dynamics (II). *Acta Math. Sci. (Engl. Ed.)* **1985**, *5*, 433–472. [CrossRef]
10. Huang, F.M.; Wang, Z. Convergence of viscosity solutions for isothermal gas dynamics. *SIAM J. Math. Anal.* **2002**, *34*, 595–610. [CrossRef]
11. Lions, P.L.; Perthame, B.; Tadmor, E. Kinetic formulation of the isentropic gas dynamics and p-systems. *Commun. Math. Phys.* **1994**, *163*, 169–172. [CrossRef]
12. Lions, P.L.; Perthame, B.; Souganidis, P. Existence and stability of entropy solutions for the hyperbolic systems of isentropic gas dynamics in Eulerian and Lagrangian coordinates. *Commun. Pure Appl. Math.* **1996**, *49*, 599–638. [CrossRef]

13. Lu, Y.G. Existence of global entropy solutions to a nonstrictly hyperbolic system. *Arch. Ration. Mech. Anal.* **2005**, *178*, 287–299. [CrossRef]
14. Shah, S.; Singh, R.; Jena, J. Steepened wave in two-phase Chaplygin flows comprising a source term. *Appl. Math. Comput.* **2022**, *413*, 126656. [CrossRef]
15. Brenier, Y. Solutions with concentration to the Riemann problem for the one-dimensional Chaplygin gas equations. *J. Math. Fluid Mech.* **2005**, *7*, S326–S331. [CrossRef]
16. Sun, M. Concentration and cavitation phenomena of Riemann solutions for the isentropic Euler system with the logarithmic equation of state. *Nonlinear Anal. Real World Appl.* **2020**, *53*, 103068. [CrossRef]
17. Chavanis, P.H. The Logotropic dark fluid as a unification of dark matter and dark energy. *Phys. Lett. B* **2016**, 758, 59–66. [CrossRef]
18. Evans, L.C. *Partial Differential Equations*, 2nd ed.; American Mathematical Society: Providence, RI, USA, 2010; p. xxii+749.
19. Mercier, J.M.; Piccoli, B. Admissible Riemann solvers for genuinely nonlinear p-systems of mixed type. *J. Differ. Equations* **2002**, *80*, 395–426. [CrossRef]
20. Fan, H.; Slemrod, M. The Riemann problem for systems of conservation laws of mixed type. In *Shock Induced Transitions and Phase Structures in General Media*; The IMA Volumes in Mathematics and its Applications; Springer: New York, NY, USA, 1993; Volume 52, pp. 61–69.
21. Slemrod, M. Admissibility criteria for propagating phase boundaries in a van der Waals fluid. *Arch. Rational Mech. Anal.* **1983**, *81*, 301–315. [CrossRef]
22. Shearer, M. The Riemann problem for a class of conservation laws of mixed type. *J. Differ. Equations* **1982**, *46*, 426–443. [CrossRef]
23. Thanh, M.D.; Vinh, D.X. The Riemann problem for van der Waals fluids with nonclassical phase transitions. *Hokkaido Math. J.* **2021**, *50*, 263–295. [CrossRef]
24. Lax, P.D. Hyperbolic systems of conservation laws. *Commun. Pure Appl. Math.* **1957**, *10*, 537–566. [CrossRef]
25. Liu, T.P. The Riemann problem for general system of conservation laws. *J. Differ. Equations* **1975**, *18*, 218–234. [CrossRef]
26. Azevedo, A.V.; Marchesin, D. Multiple viscous profile Riemann solutions in mixed elliptic-hyperbolic models for flow in porous media. In *Nonlinear Evolution Equations that Change Type*; The IMA Volumes in Mathematics and its Applications; Springer: New York, NY, USA, 1990; Volume 27, pp. 1–17.
27. Azevedo, A.V.; Marchesin, D.; Plohr, B.; Zumbrun, K. Capillary instability in models for three-phase flow. *Z. Angew. Math. Phys.* **2002**, *53*, 713–746. [CrossRef]
28. Chalons, C.; Coquel, F.; Engel, P.; Rohde, C. Fast relaxation solvers for hyperbolic-elliptic phase transition problems. *SIAM J. Sci. Comput.* **2012**, *34*, A1753–A1776. [CrossRef]
29. He, F.; Wang, Z.; Chen, T. The Shock Waves for a Mixed-Type System from Chemotaxis. *Acta Math. Sci. Ser. B (Engl. Ed.)* **2023**, *43*, 1717–1734. [CrossRef]
30. Holden, H. On the Riemann problem for a prototype of a mixed type conservation law. *Commun. Pure Appl. Math.* **1987**, *40*, 229–264. [CrossRef]
31. Hsiao, L.; De Mottoni, P. Existence and uniqueness of the Riemann problem for a nonlinear system of conservation laws of mixed type. *Trans. Am. Math. Soc.* **1990**, *322*, 121–158. [CrossRef]
32. Keyfitz, B.L.; Sanders, R.; Sever, M. Lack of hyperbolicity in the two-fluid model for two-phase incompressible flow. *Discret. Contin. Dyn. Syst. Ser. B* **2003**, *3*, 541–563. [CrossRef]
33. Li, T.; Liu, H.; Wang, L. Oscillatory traveling wave solutions to an attractive chemotaxis system. *J. Differ. Equations* **2016**, *261*, 7080–7098. [CrossRef]
34. Li, T.; Mathur, N. Riemann problem for a non-srtrictly hyperbolic system in chemotaxis. *Discret. Contin. Dyn. Syst. Ser. B* **2022**, *27*, 2173–2187. [CrossRef]
35. Mailybaev, A.A.; Marchesin, D. Lax shocks in mixed-type systems of conservation laws. *J. Hyperbolic Differ. Equ.* **2008**, *5*, 295–315. [CrossRef]
36. Medeiros, H.B. Stable hyperbolic singularities for three-phase flow models in oil reservoir simulation. *Acta Appl. Math.* **1992**, *28*, 135–159. [CrossRef]
37. Smoller, J. *Shock Waves and Reaction-Diffusion Equations*, 2nd ed.; Springer: New York, NY, USA, 1994.
38. Gottlieb, D.; Shu, C.W. On the Gibbs phenomenon and its resolution. *SIAM Rev.* **1997**, *39*, 644–668. [CrossRef]
39. Hsiao, L. Uniqueness of admissibel solutions of Riemann problem of systems of conservation laws of mixed type. *J. Differ. Equations* **1990**, *86*, 197–233. [CrossRef]
40. Jiang, G.S.; Shu, C.W. Efficient implementation of weighted ENO schemes. *J. Comput. Phys.* **1996** *126*, 202–228. [CrossRef]
41. Shearer, M. Nonuniqueness of admissible solutions of Riemann initial value problems for a system of conservation laws of mixed type. *Arch. Ration. Mech. Anal.* **1986**, *93*, 45–59. [CrossRef]